Bulletin of the Seismological Society of America, Vol. 84, No. 3, pp. 817–825, June 1994

Southern Surface Rupture Associated with the *M* 7.3 1992 Landers, California, Earthquake

by S. E. Hough

Abstract Although most evidence suggests that the 28 June 1992 *M* 7.3 Landers earthquake ruptured unilaterally north, significant surface rupture was mapped on the Eureka Peak and Burnt Mountain faults, to the south of the Landers epicenter. An eyewitness account reports that surface rupture occurred on the northern Eureka Peak fault within approximately 35 sec of the mainshock initiation. Array analysis of the Landers mainshock provides evidence in support of this report; a significant southern subevent in the early mainshock coda. I also analyze dense array recordings of a *M* 5.6 aftershock that occurred 3 min after the mainshock at 34°7.65′N, 116°23.82′W and show that there is strong evidence that this event was also associated with significant rupture on the Eureka Peak fault. This analysis thus suggests that the Eureka Peak fault rupture was not caused by direct bilateral mainshock rupture but instead was initially triggered less than a minute after the mainshock and reruptured by the *M* 5.6 aftershock. Results for the evolution of the Landers sequence suggest that mainshock subevents may in some cases be accurately described as aftershocks (i.e., disjoint triggered events) that occur within the duration of mainshock strong ground motion.

Introduction: Data

Three days after the magnitude 6.1 22 April Joshua Tree, California, earthquake (Fig. 1), we deployed portable digital GEOS recorders (Borcherdt *et al.*, 1985) with Mark Products L-22 2-Hz sensors and Kinemetrics force-balance accelerometers (FBA's) at eight sites. The data were sampled at 200 samples per second on all channels. Four of the instruments were deployed in a dense array in the Morongo Valley, with station spacings of 300 to 500 m. Five of the eight sites, including three in Morongo Valley, were operating at the time of the 11:57:34 28 June Landers, California, mainshock (Fig. 1). The Landers event occurred at 34°12′N, 116°26′W, and is associated with 70 km of surface rupture to the north of the epicenter (Sieh *et al.*, 1993). The mainshock and its early aftershocks, including a *M* 5.6 event in Yucca Valley that occurred 3 min after the mainshock, were recorded on-scale by the FBA's at all five sites.

The three operating Morongo Valley sites were all located within 1 km of each other, on sedimentary sites toward the edge of the valley. The edge of the valley runs parallel to the Morongo Valley fault mapped on Figure 1; the approximate valley edge is indicated in the inset with a dashed line. Peak accelerations of approximately 0.19 to 0.31 *g* and 0.077 to 0.115 *g* were recorded for the mainshock and aftershock, respectively, on the three array sites, MVB, MVH, and MVP (Fig. 2a). At MVP, we recovered only the north–south horizontal FBA component; at MVB and MVH we recovered all three components.

The *M* 5.6 aftershock, henceforth referred to as the Yucca Valley aftershock, is located by the Southern California Seismic Network (SCSN) at 34°8′N, 116°24′W with a shallow hypocentral depth. The network location is consistent with a relocated epicenter, 34°7.65′N, 116°23.82′W, obtained by Hauksson *et al.* (1992) using calibration shot data. The uncertainty in the relocated epicenter is estimated to be 0.5 to 1 km (Hauksson, personal comm.). Although the Yucca Valley event closely follows the Landers mainshock, the location is relatively well resolved because the coda had died down sufficiently on the SCSN strong-motion stations to permit good identification of arrivals. While the relocated hypocentral depth, estimated at ~1 km, is not as well constrained, it suggests that the event probably was quite shallow.

The location of the Yucca Valley event, the concentration of early aftershocks south of the mainshock epicenter, and the observed surface rupture to the south of the mainshock epicenter are somewhat surprising given evidence that the Landers earthquake ruptured

unilaterally to the north (Wald *et al.*, 1992). Although stress concentration at the ends of an earthquake rupture is expected, a primary mainshock rupture is generally assumed to be delineated by the very early aftershocks.

Surface rupture south of Yucca Valley was mapped following the Landers earthquake (USGS/CDMG Staff, 1992), beginning just southeast of the town of Yucca Valley and continuing at approximately 160° azimuth for ~11 km, with a maximum horizontal displacement of 20 cm. No previous surface rupture was observed in this area following the earlier 22 April 1992 M 6.1 Joshua Tree earthquake (Rymer, 1992). This fault was previously unrecognized and has been named the Eureka Peak fault (Rymer, 1992; Treiman, 1992). A resident of Yucca Valley, Mr. Shultz, reports being woken up by the mainshock, running outside, and watching a rupture propagate through his yard after being outside for approximately 15 to 20 sec. This rupture has been identified as being part of the Eureka Peak fault. Surface rupture was also mapped on the nearby Burnt Mountain fault, with a maximum right-lateral displacement of 6 to 7 cm observed over ~2 km (Fig. 1b).

Array analysis of the Yucca Valley aftershock is presented by Hough *et al.* (1993); in this article, we present a summary of those results and array analysis of the Landers mainshock. We focus on implications for the evolution of the southern "Landers" surface rupture.

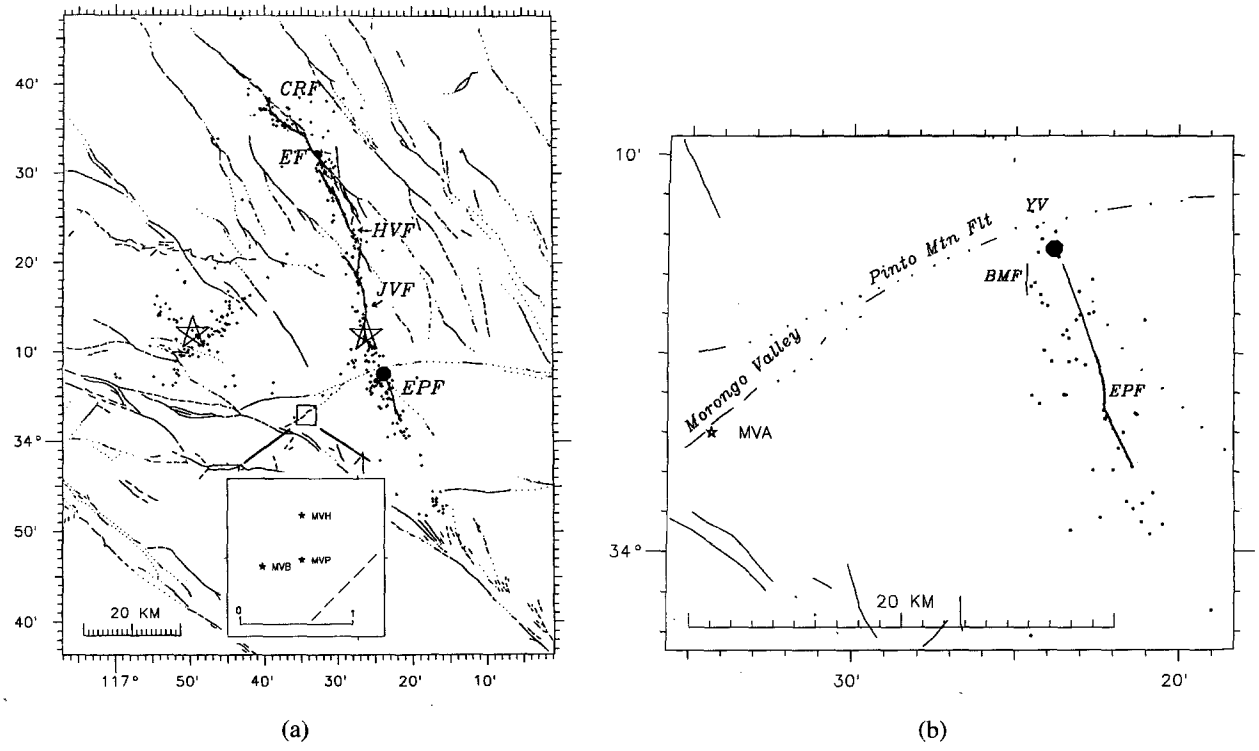

Figure 1. A map of the southern Landers aftershock zone showing the locations of all $M \geqq 3$ aftershocks located through 29 June 1992 (dots), the Landers and Big Bear epicenters (stars), the epicenter of the Yucca Valley aftershock (large circle), the mapped surface rupture north and south of the Pinto Mountain Fault (heavy lines), and the location of the Morongo Valley dense array. The Eureka Peak, Johnson Valley, Homestead Valley, Emerson, and Camp Rock faults are indicated by EPF, JVF, HVF, EF, and CRF, respectively. Base map shows quaternary faults. Inset shows detailed geometry of Morongo Valley stations, MVP, MVB, and MVH. The inset scale indicates 1 km; the dashed line indicates the approximate SE edge of the valley and the mapped Morongo Valley fault. The far valley edge is roughly parallel to this line, 2 to 3 km to the northwest. (b) Detailed map showing the location of the Morongo Valley dense array (MVA), the town of Yucca Valley (YV), the Yucca Valley aftershock (large circle), and the southern surface rupture. The left trace corresponds to the Burnt Mountain fault (BMF), and the right trace to the Eureka Peak fault (EPF). (The Johnson Valley rupture is north of the region shown.) Small dots again indicate early Landers aftershocks with magnitudes greater than 3.

Our results will be discussed in light of the eyewitness account.

Analysis

Methodology

High-frequency ground motions recorded during both the mainshock and the Yucca Valley event vary considerably at the three Morongo Valley array sites. Peak accelerations for the event vary by almost 50%. To investigate the possibility that the variability could be a result of instrumental differences or problems, Figure 2b presents displacements for the first ~10 sec of the Yucca Valley aftershock recorded at stations MVP and MVH. (The record at MVB is very similar to that at MVH, and is not shown.) To obtain displacement, acceleration rec-

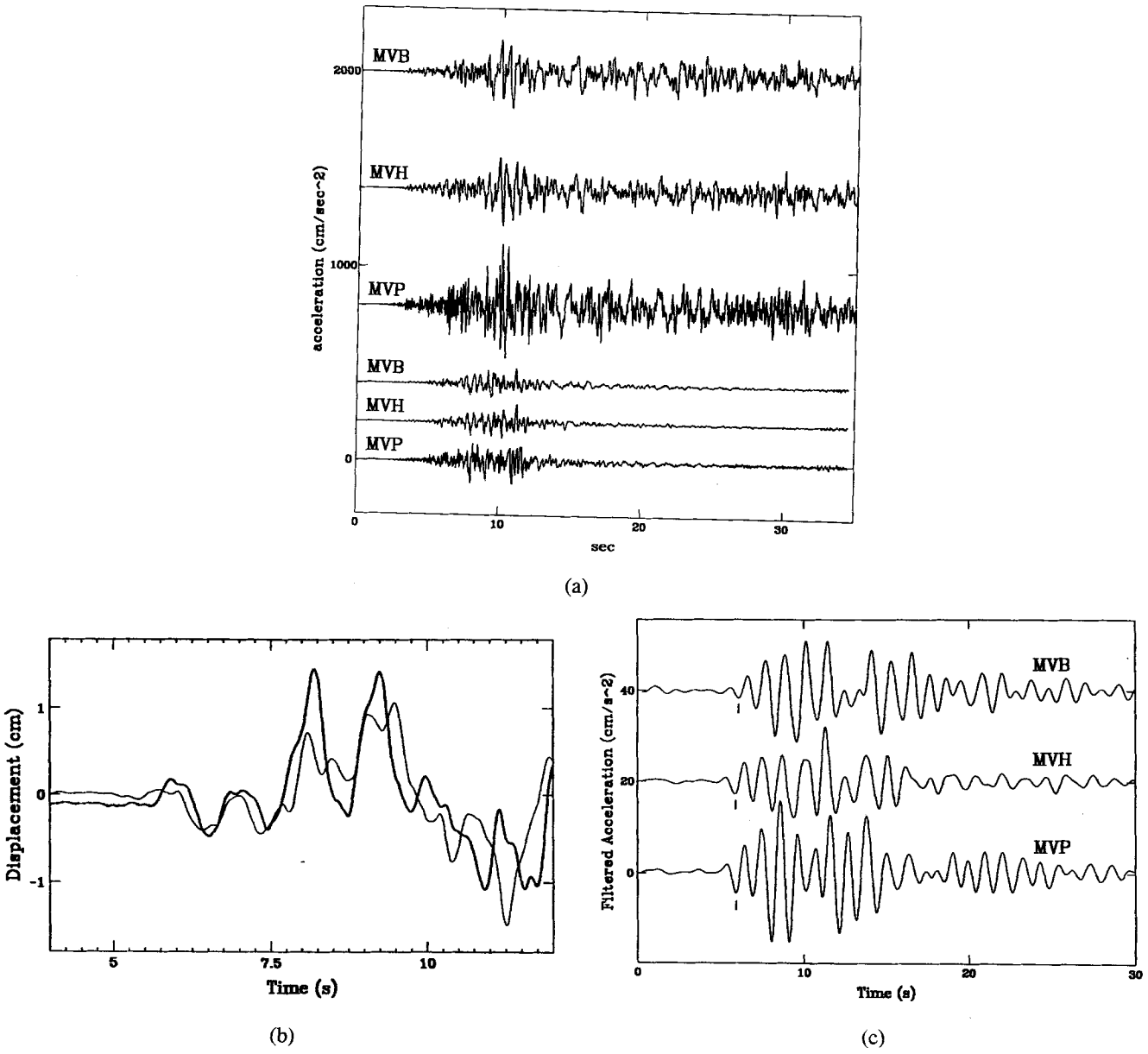

Figure 2. (a) The N–S component of ground motion recorded on strong-motion instruments at MVP, MVB, and MVH for the Landers mainshock (*top*) and the Yucca Valley aftershock (*bottom*). Records are offset for clarity. (b) Displacement records for the first −10 sec of the Yucca Valley event at stations MVP (dark line) and MVH (light line) are overlain. Acceleration records are twice integrated and high-pass filtered above 0.1 Hz to obtain displacement. (c) Accelerograms for the Yucca Valley aftershock, low-pass filtered with a corner frequency of 1 Hz. Traces are offset and, for the array analysis, are aligned along first large negative pulse (indicated) rather than by absolute time.

ords were integrated twice and high-pass filtered above 0.1 Hz. The good coherence of the displacements argues against the likelihood of instrumental problems at any of the sites. The variation in high-frequency ground motions, observed at stations within 500 m of each other with similar near-site geology, is surprisingly large and suggests that a factor of 50% uncertainty in peak acceleration may be expected even after accounting for generalized site conditions.

A good coherence is also observed in the acceleration data low-pass filtered with a corner frequency of 1 Hz (Fig. 2c). A third-order Butterworth filter is used on the north–south components at each station.

Because the absolute timing is unreliable at the level of accuracy needed to perform array analysis, and because clear arrivals are difficult to identify, the time series are aligned so that initial arrivals have an apparent velocity across the array of 1800 m/sec. This assumed apparent velocity is slower than the expected shear-wave velocity across the array. However, higher assumed apparent velocities do not yield stable results, while the same absolute time shift results in correct initial locations for both the mainshock and the Yucca Valley event. In a later section, we will show that a physical explanation can be made to account for the low apparent velocity. The process of aligning the seismograms obviates a possibly large source of timing error caused by site delays resulting from lateral variations in sediment structure.

To estimate apparent phase velocities and backazimuths of arrivals, we use a moving-window slowness analysis presented by Frankel *et al.* (1991). Using filtered, windowed seismograms, cross correlations

$$C = \frac{\Sigma\,[x_1(t + \delta t)x_2(t)]}{\sqrt{\Sigma\,[x_1(t + \delta t)^2]\,\Sigma\,[x_2(t)^2]}} \tag{1}$$

are determined for a range of time delays,

$$\delta t = p_x \delta x + p_y \delta y, \tag{2}$$

where the east–west and north–south slowness, p_x and p_y, respectively, vary over a range of values. The average cross correlation is determined for all pairs of stations, and the p_x and p_y values for a given time window are determined to be those values that give a maximum average cross correlation for all pairs. The apparent horizontal velocity across the array is then given by

$$V = \frac{1}{\sqrt{p_x^2 + p_y^2}} \tag{3}$$

and the backazimuth ϕ is

$$\phi = \tan^{-1}(p_x/p_y). \tag{4}$$

Backazimuth and slowness estimates can be made for overlapping windows through the duration of the strong ground motion: in a later section we will discuss the estimation of uncertainties.

The Landers Mainshock

We experimented with a variety of data processing methods for the mainshock data and conclude that, for this case, the most stable results are obtained using doubly integrated acceleration records that have been high-pass filtered above 0.2 Hz. Results obtained with either acceleration or displacement records filtered above 0.1 Hz are somewhat less stable, but basically consistent, and will not be shown. To align the time series, we use the same absolute time shift that will be used for the Yucca Valley aftershock. We also tried a number of alternative alignments and conclude that they yield less stable results, thus providing an added measure of confirmation of the alignment.

The filtered displacement records used for array analysis are shown in Figure 3. For this analysis, subwindows 2.5-sec long are used, with a translation of 1 sec. The results are shown in Figure 4 for all subwindows for which a correlation of 0.7 is obtained. The choice of a minimum cutoff is subjective but made based on an assessment of the minimum correlation value for which results appear to be stable.

Figure 4 suggests that, between 9 and 22 sec (relative to an arbitrary origin shown in Fig. 3), energy arrives from a backazimuth consistent with that of the known epicenter and southern surface rupture. Between 22 and 28 sec, energy arrives from a more northerly (N-NNW) direction, consistent with the backazimuth to the Emerson-Camp Rock faults on which the maximum surface displacement was observed. Between 29 and 31 sec, energy arrives from almost due east. Between 31 and 39 sec, low correlations are generally obtained, except for

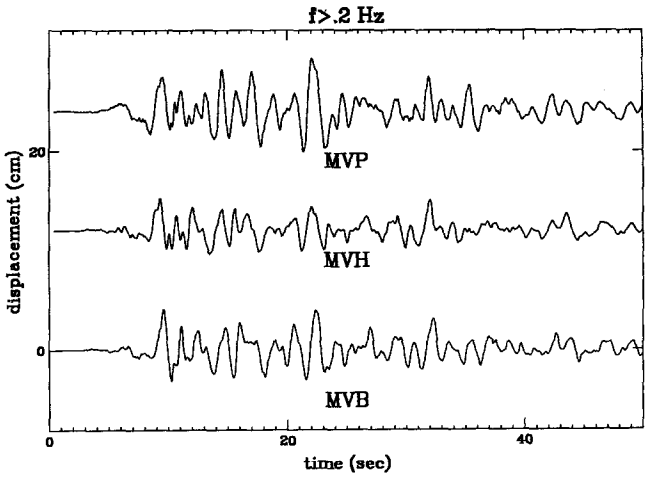

Figure 3. Mainshock displacement records obtained by twice-integrating the recorded accelerations and high-pass filtering above 0.2 Hz.

34 to 35 sec, for which a northerly backazimuth is obtained. Between 39 and 45 sec, a backazimuth of roughly due east is again obtained.

Apparent velocities are consistently scattered around ~1600 m/sec. These values are somewhat lower than the expected apparent *S*-wave velocity across the array if the arrivals in Morongo Valley are refracted from a higher velocity layer at depth (in which case the apparent velocity should be the *S*-wave velocity at depth). The sediment-basement interface under the Morongo Valley array dips towards the west, however, and theoretical finite-difference modeling results show that significant decreases in apparent velocities result from this geometry (Frankel and Vidale, 1994). Arrivals further into the valley have longer travel paths through the slow near-surface layer, biasing the apparent velocities toward low values. If the arrivals in Morongo Valley are direct rays, then the expected apparent velocity will be the near-surface *S*-wave velocity, in which case 1600 to 1700 m/sec is also reasonable. For a few time windows, low apparent velocities may indicate surface-wave arrivals, although as we will discuss, the uncertainties associated with the apparent velocity estimates are considerable.

Error bars for the backazimuth results can be obtained from the range of backazimuths that yield correlations within a certain percentage of the maximum value. A geometrical description of this procedure is illustrated in Figure 5, which presents slowness contours for a time window beginning 41 sec into the mainshock record. Error bars can be obtained similarly for the apparent velocity estimates, and are shown in Figure 5. The elongation of the contours along the NW direction reflects the fact that the array is somewhat "flattened" in this direction, yielding relatively poor resolution. The apparent velocities are observed to be considerable, with error bars typically spanning spreads of 800 to 1400 m/sec.

In choosing the range of acceptable correlations, we have focused on subwindows in which first-order patterns of arrivals across the array can be used to constrain the backazimuth with some confidence. We conclude that correlations as low as approximately 95% of the maximum yield a range in backazimuths that is consistent with first-order observations. We use the same criterion to ob-

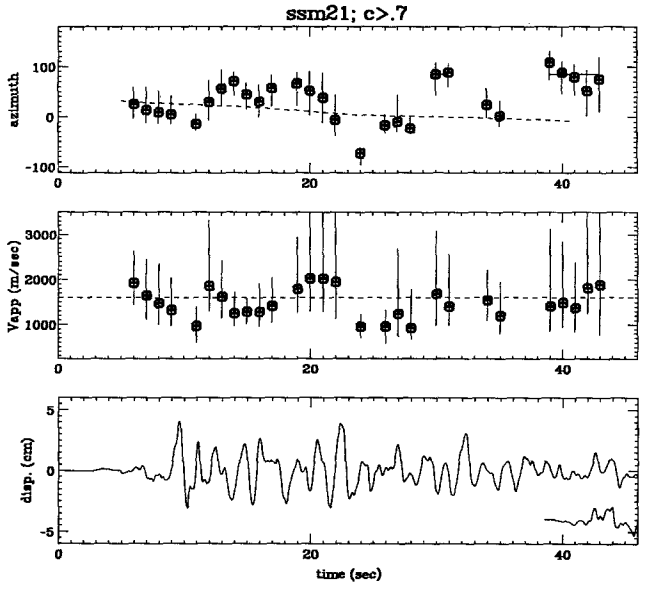

Figure 4. Backazimuth (*top*) and apparent velocity (*middle*) results for all subwindows of the Landers mainshock for which correlations of at least 0.7 are obtained. The backazimuth error bars are estimated according to the procedure illustrated in Figure 5, the dashed line indicates the expected backazimuths for a smooth rupture along the mapped surface faults, and the solid line indicates the average backazimuth observed between 39 and 43 sec. The dashed line in the middle figure indicates a rough average of the inferred apparent velocities: 1600 m/sec. In the bottom figure, the filtered displacement record at MVB is shown along with an offset displacement trace at the same station from the Yucca Valley aftershock.

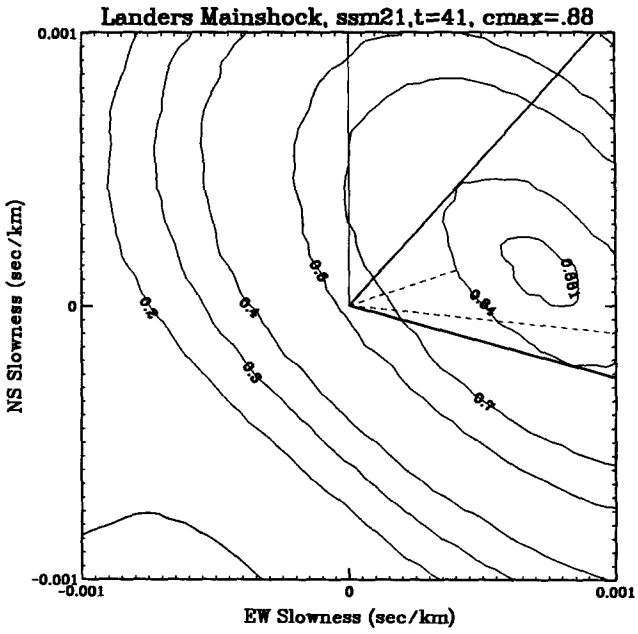

Figure 5. Correlation values are contoured as a function of N–S and E–W slowness across the array for a 2.5-sec subwindow beginning 41 sec into the mainshock record shown in Figure 3. The dark lines indicate the range of backazimuths that are consistent with correlations that are ≧95% of the maximum observed values (with azimuth measured clockwise from north, indicated by light line). The corresponding range of apparent velocities can be calculated from the corresponding range of distances from the origin (dashed lines). In this case, the maximum slowness is off of the plot.

tain error bounds for each time window; these are shown in Figure 4.

Although the backazimuth uncertainties are large, there does appear to be significant differences between the different time windows. Averaging the inferred backazimuths for the four subwindows 9 to 20, 22 to 28, 29 to 31, and 39 to 45 sec, we obtain backazimuths (respectively) of: 37.4 ± 23.3°, −9.5 ± 7.4°, 84.6 ± 3.7°, and 88.5 ± 17.6°. In the discussion, we will refer to time windows I through IV corresponding to these four intervals.

The Yucca Valley Aftershock

An analysis of the Yucca Valley aftershock is presented in Hough *et al.* (1993); the results are summarized here. In this case, low-pass filtered acceleration records are used. Results using displacement records are generally consistent, but somewhat less stable, possibly as a result of the presence of long-period waves from the Landers coda. For this analysis, we use 0.5-sec windows whose centers are translated by steps of 0.3 sec. A 50 by 50 grid of slowness values is used with increments of 0.02 sec/km, corresponding to a slowness range of ±1 sec/km.

Figure 6 summarizes the final results values for the filtered acceleration records for all time windows for which the maximum correlation is at least 0.99. Notably, the backazimuths vary from approximately 65° at the start of the *S* arrivals to −105° 4 sec later. Assuming these waves to be direct arrivals, this indicates a north-to-south propagation of the rupture. Between t = 8.4 and t = 10 sec, the apparent velocities drop from −1700 to −1100 m/sec.

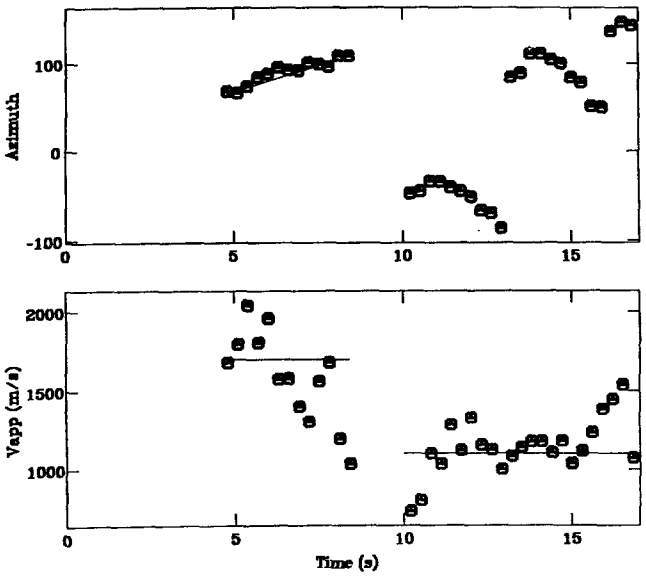

Figure 6. The bottom figure shows the inferred apparent velocities calculated for 0.5-sec subwindows throughout the recording; the top figure shows the inferred backazimuths calculated for the same subwindows. The solid lines are fit by eye, for illustration.

Error bars are not calculated for this event because a demonstration of the significance of the backazimuth shift can be seen without consideration of formal uncertainties; in Figure 2b, early in the record, the *S* waves arrive first at station MVH to the north, while later they arrive first at station MVP to the south. This observation requires a north-to-south propagation of significant duration to produce the observed shift, as discussed more quantitatively in a following section.

The apparent velocities of the main arrivals again cluster around 1600 to 1700 m/sec, close to the assumed initial apparent velocity across the array. Arrivals after 10 sec are characterized by low apparent velocities and inferred to be surface waves generated at the edge of the Morongo Valley, as discussed by Hough *et al.* (1993).

Interpretation of Results

The Landers Mainshock

During time window I, array results are consistent with energy arriving from the Johnson Valley fault on which the mainshock initiated (Fig. 1). The resolution is not good enough to discern details of rupture propagation within this interval. Starting near 22 sec, or roughly 17 sec after the mainshock initiation, energy is inferred to arrive from slightly west of north, from a backazimuth consistent with that of the Emerson-Camp Rock (E-CR) faults.

One source of uncertainty in the interpretation results from possible contributions to the waveforms from surface-wave arrivals, either converted surface waves generated in the Morongo Valley sediments (e.g., Frankel *et al.*, 1991) or longer-period crustal surface waves. The restriction to periods shorter than 5 sec should eliminate most of the latter, while the former remains a more possible complication. As discussed above, low apparent velocities are diagnostic of converted basin surface waves. Figure 4 illustrates that there are several time windows for which the inferred apparent velocities might be consistent with converted surface-wave arrivals, most notably near 25 sec.

Although the resolution is therefore limited, the results do suggest some body-wave arrivals from a N-NNW backazimuth between 22 and 35 sec, and these results can be compared with detailed mainshock rupture results from other studies (e.g., Wald *et al.*, 1992; Campillo and Archuleta, 1992). The maximum surface rupture during the Landers earthquake occurred in what is considered a second subevent of the mainshock, along the Emerson fault, approximately 30 km north of the mainshock epicenter. The mainshock is known to have propagated northward (e.g., Kanamori *et al.*, 1992), and

it is most likely that triggered rupture on the E-CR faults occurred only when the rupture front reached those faults. In Morongo Valley, energy from the E-CR faults will arrive after a delay equal to the rupture duration from the epicenter to the southernmost Emerson fault plus the extra propagation time back to Morongo Valley. Assuming a maximum plausible rupture velocity of 3 km/sec, the rupture propagation would require on the order of 10 sec. Propagation of energy back toward Morongo Valley can be estimated from the distance (30 km) and the propagation velocity, conservatively bounded at 4 km/sec for shear waves. Thus, the inferred delay of 17 sec appears to represent a lower bound for the time delay required for energy from the E-CR fault to reach Morongo Valley. The results presented here are consistent with more detailed studies of the mainshock rupture propagation (Wald *et al.*, 1992; Cohee and Beroza, 1994) that argue against any appreciable time delay (i.e., more than 1 to 2 sec) between the two primary mainshock subevents. The resolution of the array analysis is not good enough to provide a test of theoretical models for dynamic fault segmentation (e.g., Harris and Day, 1993), which predict some slowing of the rupture front as it propagates across steps.

During time windows III and IV, energy arrives at the array from approximately due east of the array. The results for time window IV are the more convincing of the two, with easterly backazimuths observed over a longer time window. Based on the array results and the eyewitness account, we conclude that a subevent occurred on the Eureka Peak fault approximately 35 sec after the mainshock initiation. The array results suggest that the 35-sec subevent continued for several seconds, suggesting a probable rupture over the entire 11 km. More speculatively, it is possible that the arrivals in time window III represent rupture on the Burnt Mountain fault.

Although a presentation of additional strong-motion data is beyond the scope of this article, Cohee and Beroza (1994) also note the suggestion of late, unmodeled energy at several stations to the south of the Landers epicenter. The timing of these arrivals is consistent with the timing and location of the subevent inferred in this study.

The Yucca Valley Aftershock

A strong, systematic variation in backazimuth is observed throughout the duration of the strong ground motion from the Yucca Valley aftershock at the Morongo Valley array. The key result—that rupture propagated from north to south—is corroborated with the discussed *prima facie* evidence: the shift in relative arrival times at two stations that are broadside to the rupture.

The results for the *S*-wave arrivals do not uniquely constrain the rupture dimensions of the Yucca Valley aftershock. However, based on both its epicentral location at the northernmost terminus of the Eureka Peak fault and a striking similarity between mainshock time window IV and the aftershock displacements (Fig. 4), we conclude that this aftershock was also most likely caused by rupture on the Eureka Peak fault.

As discussed by Hough *et al.* (1993), a rupture duration for the aftershock can be inferred by assuming the end of the dynamic rupture coincides with the time at which the apparent phase velocity across the array drops and the inferred converted surface waves arrive. Hough *et al.* (1993) infer an azimuthal variation of ~40° (65 to 105) over approximately 3.6 sec. Projecting this range onto a N–S rupture initiating 16 km away yields a length of 10.9 km [and a rupture velocity of 3 km/sec; within the expected range (Boatwright, 1982)], almost exactly the length of the observed surface rupture. The primary uncertainty in estimating this rupture length results from uncertainty in the ending backazimuth of the arrivals. Estimates of both slowness and backazimuths become somewhat unstable near the inferred rupture end, probably as a result of interference between the end of the direct arrivals and the beginning of converted surface-wave arrivals. Assuming a plausible azimuthal range of 30° to 50°, rupture lengths of 8.3 to 13.6 km are obtained.

If we assume that the mapped surface fault ruptured over an area of 11 by 8 km, with an average slip of 18 cm and a shear modulus of 3×10^{11} dyne · cm, the estimated moment for this rupture is 4.8×10^{24} dyne · cm. This is equivalent to a moment magnitude (M_w) of 5.8 (Thatcher and Hanks, 1973; Hanks and Kanamori, 1979). Geodetic inversions suggest a higher slip for the Eureka Peak fault, on the order of 20 to 50 cm (D. Jackson, personal comm.). Thus, it may be that slip at depth is considerably higher than at the surface, and that the total inferred from geodetic data is consistent with two magnitude ~5.6 ruptures.

Discussion

Array analysis of the Landers mainshock corroborates an eyewitness account whose veracity was difficult to assess independently. The eyewitness observations are inconsistent with immediate bilateral mainshock rupture because the Landers mainshock is less than 10 km north of Yucca Valley and should have produced primary rupture within 3 to 4 sec.

The analysis presented here leads to the following scenario for the southern Landers surface rupture: 30 sec after the mainshock initiation, rupture on the Burnt Mountain fault to the south of the epicenter may have triggered approximately 30 sec after the mainshock initiation. This timing shortly follows the arrival of energy from the Emerson-Camp Rock rupture, suggesting that the large dynamic surface-wave strains associated with the second mainshock subevent may have triggered the Burnt Mountain fault rupture. Approximately 5 sec after

this, rupture was triggered on the Eureka Peak fault. We cannot resolve whether this rupture propagated N-to-S or S-to-N (the array results favor the latter, but are not conclusive), but the results suggest that this subevent involved the entire length of the 11-km surface rupture.

Approximately 3 min after the Landers mainshock initiation, the Eureka peak fault reruptured (resolvably N-to-S) over its entire length during the *M* 5.6 Yucca Valley aftershock. Near-instantaneous rerupture of faults has been inferred in previous earthquakes, such as the 1987 Superstition Hills earthquake (Wald *et al.*, 1990) and the 1985 Nahanii earthquakes (Wetmiller *et al.*, 1988). This phenomenon is inconsistent with classical fault models in which stresses are completely released by earthquake rupture, but can be explained within the confines of the abruptly healing slip pulse model proposed by Heaton (1990). According to this model, earthquake rupture does not necessarily result in complete stress drop, and near-instantaneous rerupture can occur. The Eureka Peak fault is roughly bounded to the south by the 1992 Joshua Tree rupture and to the north by the 1992 Landers rupture; the inferred slip over the Eureka Peak fault is less than what occurred on both sides. Thus, it is plausible that considerable residual stress continued to exist after a first rupture of the fault. It is interesting to note that the only appreciable postseismic creep observed along the Landers mainshock rupture occurred along the Eureka Peak fault (P. Bodin, personal comm.), providing further evidence for residual stress.

Our results also provide grist for speculation concerning the nature of large earthquake rupture. Although the simplest conceptual model is one in which rupture begins at a point and propagates continuously in one direction (or bilaterally), detailed investigations of earthquake rupture reveal that many earthquakes can be regarded as separate subevents, with the first of these triggering those that follow (e.g., Mendez and Anderson, 1991; Kanamori *et al.*, 1994; Pacheco *et al.*, 1989). These subevents sometimes follow an orderly progression along strike of the rupture (e.g., Kanamori *et al.*, 1994), but our results suggest that the large dynamic (and possibly static) strains associated with large earthquake rupture can trigger disjoint subevents that are essentially aftershocks that occur before the "mainshock" strong ground motion is over.

Similar early triggered events have been inferred for other events as well, with time delays ranging from 11.4 hr (The 1987 Superstition Hills, California, sequence; Hudnut *et al.*, 1989), to 4 to 5 sec for distinct faulting events inferred during the 28 June 1992 *M* 6.5 Big Bear earthquake (itself considered an aftershock of Landers; Jones and Hough, 1994). Given the dynamic and static stress changes associated with large earthquakes (e.g., Rice and Cleary, 1976; Reasenberg and Simpson, 1992; Hill *et al.*, 1993), it is perhaps not surprising that an earthquake as large as Landers will be associated with significant secondary events. This type of complex rupture scenario transcends the usual taxonomy of "foreshocks," "mainshocks," and "aftershocks": instead, phenomena such as disjoint mainshock subevents emerge as manifestations of a continuum of triggered effects related to static and dynamic changes caused by earthquake rupture.

Conclusions

We have used array analysis of strong-motion recordings of the *M* 7.3 Landers mainshock and the *M* 5.6 Yucca Valley aftershock to investigate the evolution of the southern "Landers" rupture. Surface rupture on the Eureka Peak and Burnt Mountain faults can be plausibly associated with distinct events that occur in the immediate wake of the primary mainshock rupture to the north. We conclude that the Eureka Peak fault ruptured twice, first approximately 35 sec after the mainshock initiation and again approximately 2.5 min later.

Acknowledgments

E. Sembera, G. Glassmoyer, C. Mueller, and S. Lydeen are gratefully acknowledged for their efforts in instrument deployment, maintenance, and data playback. I acknowledge the cooperation and patience of C. Schultz, G. Whitney, R. Skaggs, and the employees of the Morongo Valley Community Center, and thank J. Treiman, M. Rymer, A. Frankel, J. Mori, P. Spudich, K. Sieh, and D. Eberhart-Phillips for helpful discussions, Egill Hauksson for providing his event relocation for the Yucca Valley aftershock, and P. Bodin for calling attention to the southern rupture mapping efforts by J. Treiman. I thank D. Wald for his review of the article, and an anonymous reviewer for helpful criticisms.

References

Boatwright, J. (1982). A dynamic model for far-field acceleration, *Bull. Seism. Soc. Am.* **72**, 1049–1068.

Borcherdt, R. G., J. B. Fletcher, E. G. Jensen, L. Maxwell, J. R. Van Shaak, R. E. Warrickm, E. Cranswick, J. S. Johnston, and R. McClearn (1985). A general earthquake-observation system, *Bull. Seism. Soc. Am.* **75**, 1783–1825.

Campillo, M. and R. J. Archuleta (1992). A rupture model for the 28 June 1992 Landers, California, earthquake (abstract) *EOS* **73**, 374.

Cohee, B. P. and G. Beroza (1994). Slip distribution of the 1992 Landers earthquake and its implications for earthquake source mechanics, *Bull Seism. Soc. Am.* **84**, no. 3, 692–712.

Frankel, A., S. Hough, P. Friberg, and R. Busby (1991). Observations of Loma Prieta Aftershocks from a dense array in Sunnyvale, California, *Bull. Seism. Soc. Am.* **81**, 1900–1922.

Frankel, A. and J. Vidale (1992). A three-dimensional simulation of seismic waves in the Santa Clara Valley, California, from a Loma Prieta aftershock, *Bull. Seism. Soc. Am.* **82**, 2045–2074.

Hanks, T. C. and H. Kanamori (1979). A moment-magnitude scale, *J. Geophys. Res.* **84**, 2348–2350.

Harris, R. A. and S. M. Day (1993). Dynamics of fault interaction: parallel strike-slip faults, *J. Geophys. Res.* **98**, 4461–4472.

Hauksson, E., K. Hutton, H. Kanamori, S. Bryant, H. Qian, K. Douglass, L. M. Jones, D. Eberhart-Phillips, J. Mori, and T.

Heaton (1992). Overview of the 1992 (M 6.1, 7.5, 6.6) Landers earthquake sequence in San Bernardino County, California, *Trans. Am. Geophys. U.* **73**, 357.

Heaton, T. (1990). Evidence for and implications of self-healing pulses of slip in earthquake rupture, *Phys. Earth Planet. Interiors* **64**, 1–20.

Hill, D. P., P. A. Reasenberg, A. Michael, W. J. Arabasz, G. Beroza, J. N. Brune, D. Brumbaugh, R. Castro, S. Davis, D. dePolo, W. L. Ellsworth, J. Gomberg, S. Harmsen, L. House, S. M. Jackson, M. Johnston, L. Jones, R. Keller, S. Malone, L. Munguia, S. Nava, J. C. Pechmann, A. Sanford, R. W. Simpson, R. S. Smith, M. Stark, M. Stickney, A. Vidal, S. Walter, V. Wong, and J. Zollweg (1993). Seismicity in the Western United States remotely triggered by the M 7.4 Landers, California, earthquake of June 28, 1992, *Science* **260**, 1617–1623.

Hough, S. E., J. Mori, E. Sembera, G. Glassmoyer, C. Mueller, and S. Lydeen (1993). Southern surface rupture associated with the 1992 M 7.4 Landers earthquake: did it all happen during the mainshock? *Geophys. Res. Lett.* **20**, 2615–2618.

Hudnut, K. W., L. Seeber, and J. F. Pacheco (1989). Cross-fault triggering in the November, 1987 Superstition Hills earthquake sequence, Southern California, *Geophys. Res. Lett.* **16**, 199–202.

Jones, L. E. and S. E. Hough (1994). Analysis of broadband records from the June 28, 1992 Big Bear earthquake: Evidence of a multiple-event source, *Bull. Seism. Soc. Am.* (submitted for publication).

Kanamori, H., H.-K. Thio, D. Dreger, E. Hauksson, and T. Heaton (1992). Initial investigation of the Landers, California, earthquake using TERRAScope, *Geophys. Res. Lett.* **19**, 2267–2270.

Kanamori, H., J. Mori, E. Hauksson, T. H. Heaton, L. K. Hutton, and L. M. Jones (1994). Determination of earthquake energy release and ML using TERRAscope, *Bull. Seism. Soc. Am.* **83**, 330–346.

Mendez, A. and J. G. Anderson (1991). The temporal and spatial evolution of the 19 September 1985 Michoacan earthquake as inferred from near-source ground motion models, *Bull. Seism. Soc. Am.* **81**, 844–861.

Pacheco, J. F., C. H. Estabrook, D. W. Simpson, and J. L. Nabalek (1989). Teleseismic body wave analysis of the 1988 Armenian earthquake, *Geophys. Res. Lett.* **16**, 1425–1428.

Reasenberg, P. A. and R. W. Simpson (1992). Response of regional seismicity to the static stress change produced by the Loma Prieta earthquake, *Science* **255**, 1687–1690.

Rice, J. and M. Cleary (1976). Some basic stress-diffusion solutions for fluid saturated elastic porous media with compressible constituents, *Rev. Geophys. Space Phys.*, 227–241.

Rymer, M. (1992). The 1992 Joshua Tree, California earthquake: tectonic setting and triggered slip, *Trans. Am. Geophys. U.* **73**, 363.

Sieh, K., L. Jones, E. Hauksson, K. Hudnut, D. Eberhart-Phillips, T. Heaton, S. Hough, K. Hutton, H. Kanamori, A. Lilje, S. Lindvall, S. F. McGill, J. Mori, C. Rubin, J. A. Spotila, J. Stock, H. K. Thio, J. Treiman, B. Wernicke, and J. Zachariasen (1993). Near-field investigations of the Landers earthquake sequence, April to July 1992, *Science* **260**, 171–176.

Thatcher, W. and T. C. Hanks (1973). Source parameters of southern California earthquakes, *J. Geophys. Res.* **78**, 8547–8574.

Treiman, J. (1992). Eureka Peak and Burnt Mountain faults, two "new" faults in Yucca Valley, San Bernadino County, in *Landers Earthquake of June 28, 1992, San Bernadino, California, Field Trip Guidebook: Southern California Section of the Ass. of Eng. Geologists, Annual Field Trip*, B. B. Ebersold (Editor).

United States Geological Survey/California Divisions of Mines and Geology Staff (1992). Pattern of surface ruptures associated with the June 28, 1992, Landers Earthquake (abstract), *Trans. Am. Geophys. U.* **73**, 357–358.

Wald, D. J., D. V. Helmberger, and S. H. Hartzell (1990). Rupture process of the 1987 Superstition Hills earthquake from the inversion of strong motion data, *Bull. Seism. Soc. Am.* **80**, 1079–1098.

Wald, D. J., D. V. Helmberger, and H. K. Thio (1992). On developing a single rupture model for the 1992 Landers, California earthquake consistent with static, broadband teleseismic, regional, and strong motion data sets (abstract), *Trans. Am. Geophys. U.* **73**, 358.

Wetmiller, R. J., R. B. Homer, H. S. Hasegawa, R. G. North, M. Lamontagne, D. H. Weichert, and S. G. Evans (1988). An analysis of the 1985 Nahanni earthquakes, *Bull. Seism. Soc. Am.* **78**, 590–616.

United States Geological Survey
Pasadena, California 91106

Manuscript received 28 June 1993.